The influence of magnetostatic interactions in exchange-coupled composite particles

D Vokoun, M Beleggia, M de Graef, H C Hou, C H Lai

The influence of magnetostatic interactions in exchange coupled composite particles

D. Vokoun[1], M. Beleggia[2], M. De Graef[3], H.C. Hou[4] and C.H. Lai[4]

[1]*Institute of Physics, Academy of Science of the Czech Republic, Prague*
[2]*Center for Electron Nanoscopy, Technical University of Denmark, DK-2800 Kgs. Lyngby, Denmark*
[3]*Department of Materials Science and Engineering, Carnegie Mellon University, 5000 Forbes Avenue, Pittsburgh, PA 15213-3890, USA*
[4]*Department of Materials Science and Engineering, National Tsing Hua University, Hsinchu, Taiwan.*

Abstract

Exchange coupled composite (ECC) particles are the basic constituents of ECC magnetic recording media. We examine and compare two types of ECC particles: i) core-shell structures, consisting of a hard-magnetic core and a co-axial soft-magnetic shell, and ii) conventional ECC particles, with a hard-magnetic core topped by a soft cylindrical element. The model we present describes the magnetic response of the two ECC particle types, taking into account all significant magnetic contributions to the energy landscape. Special emphasis is given to the magnetostatic (dipolar) interaction energy. We find that both the switching fields and the zero-field energy barrier depend strongly on the particle geometry. A comparison between the two types reveals that core-shell ECC particles are more effective in switching field reduction, while conventional ECC particles maintain a larger overall figure of merit.

Exchange coupled composite (ECC) magnetic recording media [1-2] have the potential to achieve ultrahigh recording densities. For instance, the recording density of dual-layer patterned media may reach up to 10 Tbit/in^2 [3]. ECC media are formed by isolated grains or particles each consisting of magnetically hard and soft parts, mutually exchange-coupled across the boundary separating them [4-6]. In the design of ECC media, particle shapes play an important role when switching field reduction and thermal stability are of concern [7].

In this study, we analyze ECC nano-dots with a basic cylindrical shape and various geometries. Each dot consists of a hard-magnetic core and either a co-axial soft-magnetic shell (core-shell ECC), or a soft-magnetic cylinder on the top of the cylindrical core (conventional ECC). By comparing the magnetic response of the two designs, we will illustrate their potential advantages and disadvantages. The magnetic response of an ECC nano-dot structure can be described in relatively simple terms under the assumption that the hard and the soft parts are uniformly magnetized due to the intrinsic ferromagnetic exchange and the small dimensions. In this case, all the significant energy terms, namely Zeeman, magnetocrystalline, interfacial exchange, and magnetostatic interactions, can be taken into account explicitly and assembled to produce the energy landscape of the system. Once the total energy is known as a function of the shape and material parameters, the magnetic behavior follows from its minimization.

Richter et al. [8] introduced a model for ECC particles that neglects magnetostatic interactions. For modeling purposes, micromagnetic simulations are generally the method of choice [7,9-10]. However, despite the increasingly faster computational resources currently available, simulations of this sort are still time-consuming, and they only allow for the exploration of the effects of varying parameters one at a time. Moreover, the cubic or tetrahedral mesh elements often used by micromagnetic software packages are ill suited for circular geometries and for defining exchange interactions on a curved surface. On the contrary, analytical micromagnetism, while seemingly oversimplified at first sight, provides an opportunity for i) capturing the essential physics of ECC particle structures and ii)

developing a broader perspective on the respective importance of the various parameters involved. In this manuscript, our main objective will be to illustrate the influence of ECC particle geometry on the magnetic response by means of analytical modeling.

To highlight the main differences between core-shell (Fig. 1a) and conventional (Fig. 1b) ECC particles, we compare their magnetic response first using a simple “two-spin” model, characterized by the simplicity of the analytical form of the energy landscape and the low dimensionality of its parameter space. Both particles have identical hard elements (C1 in Fig. 1), i.e. they are made of the same material and have equal dimensions. To investigate more deeply the magnetic response of ECC particles, we then generalize the treatment to multi-spin models, where we discretize the soft part of an ECC particle (Fig. 1) while maintaining only one additional exchange coupling parameter.

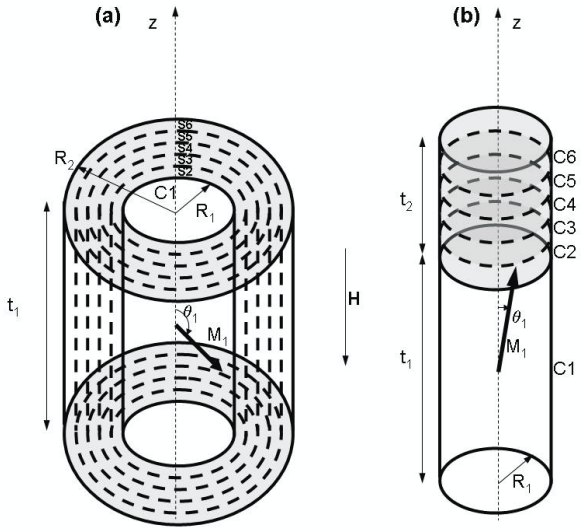

Fig. 1 Schematic of (a) a cylinder-shell nano-dot and (b) a cylinder-cylinder nano-dot and their division into spin regions (regions with uniform magnetization). Part C1 is magnetically hard; the other regions are magnetically soft.

Since the two-spin model is a special case of the multi-spin model, we will describe the latter more in detail. We assume a uniform magnetization state in each "spin" region and uniaxial anisotropy of the magnetically hard material with an easy axis parallel to the rotation axis, which also coincides with the direction of the applied field. The key elements of the model, i.e. the magnetostatic coupling between

sub-units (cylinders and shells), are described in references [11] (for core-shell interactions) and [12] (for cylinder-cylinder interactions). Following the standard Stoner-Wohlfarth approach [13], the magnetic energy of the system is minimized with respect to the magnetization vector orientation while the applied field varies. For each ECC particle type, we compute the switching fields for various strengths of exchange coupling at the interface between the soft and the hard regions. The energy minimum is determined numerically using the downhill simplex method [14], which means that we must assign specific geometric and material parameters. One of the important outputs of the model is the switching field dependence on the exchange coupling strength. From this dependence, we can determine the optimum exchange coupling strength corresponding to a maximum switching field reduction. Knowing the optimum switching field and the energy barrier at zero applied field, one can then compute a figure of merit, as defined in [4,8].

For the material and geometry parameters, we choose parameters representative of current CoCrPt based magnetic recording media: a hard cylinder radius of R_1=3 nm and a height of t_1=3,6,9,12,15 nm; the saturation magnetization of the soft material is twice that of hard material; and the coercivity of the hard cylinder is twice its saturation magnetization ($H_1 = 2M_1$, for an estimate of H_1 of a CoCrPt single grain see e.g. [15] while using $H_1 = \frac{2K_1}{M_1}$). As for the subdivision of the nano-dot into "spin regions" or domains (regions with uniform magnetization), either the soft shell/cylinder or the hard cylinder is divided into generally N coaxial shells (S2, S3, S4, S5, S6 in Fig. 1a) or cylinders (C2, C3, C4, C5, C6 in Fig. 1b). The two-spin model then corresponds to $N = 1$, and for the six-spin model we have $N = 5$.

To model the energy landscape, we express the individual magnetic contributions for each spin region, and add them together:

$$E = \sum_{i=1}^{N+1}(E_A^i + E_Z^i) + \sum_{j=1}^{N} E_x^j + \sum_{i=1}^{N}\sum_{j=i+1}^{N+1} E_d^{ij} \ , \qquad (1)$$

where E_A^i and E_Z^i are the anisotropy and Zeeman energies of the *i*-th domain, E_x^j is the exchange energy between the *j*-th and (*j*+1)-th elements, and E_d^{ij} is the dipolar interaction energy between the *i*-th and *j*-th domains. For each region *i*, we denote by V_i, S_i, N_z^i, M_i, θ_i, its volume, interfacial area, axial demagnetizing factor, saturation magnetization, and the angle between *z*-axis and magnetization direction, respectively. Finally, K_1 is the magnetocrystalline constant assigned to the hard cylinder. With such notation, and discretizing the soft part, the significant energy terms are given by:

$$E_A^i = \frac{1}{2}\mu_0 M_i^2 V_i \frac{1-3N_z^i}{2}\sin^2\theta_i - \delta_{i1}K_1 V_1 \cos^2\theta_1, \tag{2}$$

$$E_Z^i = -\mu_0 M_i V_i H\cos\theta_i, \tag{3}$$

$$E_d^{ij} = \pi\mu_0 M_i M_j R_1^3 A_{ij}(\sin\theta_i \sin\theta_j - 2\cos\theta_i\cos\theta_j), \tag{4}$$

$$E_x^i = -J_i S_i \cos(\theta_i - \theta_{i+1}), \tag{5}$$

where A_{ij} and J_i are the dipolar and exchange coupling strengths, respectively, and δ_{ij} is the Kronecker delta. The dipolar coupling factors A_{ij} depend solely on the geometry of the interacting elements. In our model, we deal with three possible types of magnetostatic interactions: cylinder-cylinder, cylinder-shell and shell-shell. Figure 2 illustrates the three kinds of shape interactions that are relevant for ECC particles. The dipolar coupling factors corresponding to the interactions between i) two coaxial cylinders of identical radius (A_{cc}), ii) a concentric cylinder and a shell of identical height (A_{cs}), and iii) two concentric shells of identical height (A_{ss}) are as follows:

$$\begin{aligned} A_{cc}(\tau_1,\tau_2,\tau_3) = \frac{1}{2}\big[&(\tau_1+\tau_3)N_z(\tau_1+\tau_3) + (\tau_2+\tau_3)N_z(\tau_2+\tau_3) \\ &- \tau_3 N_z(\tau_3) - (\tau_1+\tau_2+\tau_3)N_z(\tau_1+\tau_2+\tau_3)\big] \end{aligned} \tag{6}$$

$$A_{cs}(\sigma_1,\sigma_2,\kappa_1,\kappa_2) = -\frac{\kappa_2}{2\sigma_2^3}\left[N_z(\kappa_2) - \sigma_2^2 N_z\left(\frac{\kappa_2}{\sigma_2}\right) - (1-\sigma_2^2)N_z^s(\sigma_2,\kappa_2)\right] + \frac{\kappa_1}{2\sigma_1^3}\left[N_z(\kappa_1) - \sigma_1^2 N_z\left(\frac{\kappa_1}{\sigma_1}\right) - (1-\sigma_1^2)N_z^s(\sigma_1,\kappa_1)\right] \tag{7}$$

$$\begin{aligned} A_{ss}(\sigma_2,\sigma_3,\sigma_4,\sigma_5,\kappa_2,\kappa_3) = &-\frac{\kappa_3}{2\sigma_4^3}\left[N_z(\kappa_3) - \sigma_4^2 N_z\left(\frac{\kappa_3}{\sigma_4}\right) - (1-\sigma_4^2)N_z^s(\sigma_4,\kappa_3)\right] \\ &+ \frac{\kappa_2}{2\sigma_5^3}\left[N_z(\kappa_2) - \sigma_5^2 N_z\left(\frac{\kappa_2}{\sigma_5}\right) - (1-\sigma_5^2)N_z^s(\sigma_5,\kappa_2)\right] \\ &+ \frac{\kappa_3}{2\sigma_4^3}\left[N_z(\kappa_3) - \sigma_3^2 N_z\left(\frac{\kappa_3}{\sigma_3}\right) - (1-\sigma_3^2)N_z^s(\sigma_3,\kappa_3)\right] \\ &- \frac{\kappa_2}{2\sigma_5^3}\left[N_z(\kappa_2) - \sigma_2^2 N_z\left(\frac{\kappa_2}{\sigma_2}\right) - (1-\sigma_2^2)N_z^s(\sigma_2,\kappa_2)\right] \end{aligned} \tag{8}$$

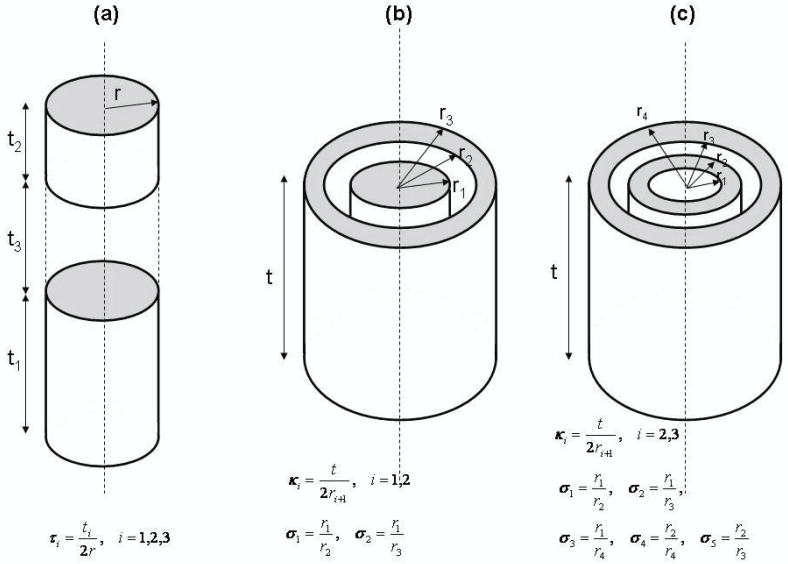

Fig. 2 Schematic of magnetostatically interacting particles of the following shapes (a) cylinder-shell (b) shell-shell and (c) cylinder-cylinder and definitions of geometric parameters.

All parameters of Equations (6-8) are defined in Fig. 2. The functions N_z and N_z^s represent the axial demagnetization factors for the cylinder and the shell, respectively [11]. Equations (6-8) were derived based on the integral form of the dipolar coupling factor, as discussed in [11] and [12]. The demagnetization factors of cylinders and shells can be expressed as combinations of elliptic integrals [11,16]. The equivalent integral forms of Equations (6-8) are as follows:

$$A_{cc}(\tau_1,\tau_2,\tau_3) = 2\int_0^\infty \frac{J_1^2(q)}{q^2}\sinh(\tau_1 q)\sinh(\tau_2 q)e^{-(\tau_1+\tau_2+2\tau_3)q}dq \tag{9}$$

$$A_{cs}(\sigma_1,\sigma_2,\kappa_1,\kappa_2) = -\frac{1}{\sigma_2^2}I(\sigma_2,\kappa_2)+\frac{1}{\sigma_1^2}I(\sigma_1,\kappa_1) \tag{10}$$

$$A_{ss}(\sigma_2,\sigma_3,\sigma_4,\sigma_5,\kappa_2,\kappa_3) = -\frac{1}{\sigma_4^2}I(\sigma_4,\kappa_3)+\frac{1}{\sigma_5^2}I(\sigma_5,\kappa_2)+\frac{\sigma_2^3}{\sigma_3^2\sigma_5^3}I(\sigma_3,\kappa_3)-\frac{\sigma_2}{\sigma_5^3}I(\sigma_2,\kappa_2), \tag{11}$$

where

$$I(\sigma,\kappa) = \int_0^\infty \frac{[J_1(q)J_1(\sigma q)-\sigma J_1^2(\sigma q)]}{q^2}(1-e^{-2q\kappa})dq \tag{12}$$

In our model, we do not employ explicitly the magnetocrystalline constant K_1; instead, we introduce the normalized coercivity of C1, $h_1 = H_1/M_1$. Since we do not discretize the hard core, we can express E_A^1 from Eq. (1) as follows:

$$E_A^1 = -\frac{1}{2}\mu_0 M_1^2 \pi R_1^2 t_1 h_1 \sin^2\theta_1, \tag{13}$$

Of the N coupling strengths associated with the N interfaces between the $N+1$ regions, J_1 reflects the exchange interaction between the hard and soft parts, while J_2 represents the exchange coupling between all soft layers ($J_3 = J_4 = ... = J_N = J_2$).

In the case of conventional ECC particles with uniformly discretized soft parts, the total energy, normalized to the factor $\mu_0 \pi R_1^3 M_1 M_2$, can be written according to Eq. (1) as

$$\begin{aligned} e_{cc} = & -\alpha\tau_1 h_1 \sin^2\theta_1 - \frac{\tau_2}{N} h_2 \sum_{i=2}^{N+1} \sin^2\theta_i + \sum_{j=2}^{N+1} \left(\sin\theta_1 \sin\theta_j - 2\cos\theta_1 \cos\theta_j\right) A_{cc}^{1j} + \\ & + \frac{1}{\alpha} \sum_{i=2}^{N} \sum_{j=i+1}^{N+1} \left(\sin\theta_i \sin\theta_j - 2\cos\theta_i \cos\theta_j\right) A_{cc}^{ij} - 2h\left(\alpha\tau_1 \cos\theta_1 + \frac{\tau_2}{N} \sum_{i=2}^{N+1} \cos\theta_i\right) \\ & - 2\sum_{i=1}^{N} J_i^r \cos\left(\theta_{i+1} - \theta_i\right) \end{aligned} \tag{14}$$

where $h = H / M_1$ is the normalized field, $\alpha = M_1 / M_2$, $\tau_i = t_i / (2R_1)$, $i = 1,2$, $h_1 = -2$,

$$h_2 = \frac{1}{2\alpha}\left[3N_z\left(\frac{\tau_2}{N}\right) - 1\right], \tag{15}$$

$$J_i^r = \frac{J_i}{2\mu_0 R_1 M_1 M_2}, \quad i = 1,2...N \tag{16}$$

and where the shape factors can be expressed according to Eq. (6) as:

$$A_{cc}^{1j} = A_{cc}\left[\tau_1, \frac{\tau_2}{N}, (j-2)\frac{\tau_2}{N}\right], \quad j = 2...N+1 \tag{17}$$

$$A_{cc}^{ij} = A_{cc}\left[\frac{\tau_2}{N}, \frac{\tau_2}{N}, (j-i-1)\frac{\tau_2}{N}\right], \quad i = 2,3...N, \quad j = 3,4...N+1 \tag{18}$$

For a core-shell ECC particle with uniformly discretized soft part, the total normalized energy is:

$$\begin{aligned} e_{cs} = & -\alpha\tau_1 h_1 \sin^2\theta_1 - \tau_1 \sum_{i=2}^{N+1} \frac{\hat{R}_i^2 - \hat{R}_{i-1}^2}{\hat{R}_1^2} h_i \sin^2\theta_i + \sum_{j=2}^{N+1} \left(\sin\theta_1 \sin\theta_j - 2\cos\theta_1 \cos\theta_j\right) A_{cs}^{j} \\ & + \frac{1}{\alpha} \sum_{i=2}^{N} \frac{\hat{R}_i^3}{\hat{R}_1^3} \sum_{j=i+1}^{N+1} \left(\sin\theta_i \sin\theta_j - 2\cos\theta_i \cos\theta_j\right) A_{ss}^{ij} - 2h\tau_1\left(\alpha\cos\theta_1 + \sum_{i=2}^{N+1} \frac{\hat{R}_i^2 - \hat{R}_{i-1}^2}{\hat{R}_1^2} \cos\theta_i\right) \\ & - 8\tau_1 \sum_{i=1}^{N} \frac{\hat{R}_i}{\hat{R}_1} J_i^r \cos\left(\theta_{i+1} - \theta_i\right) \end{aligned} \tag{19}$$

where $\hat{R}_i$ are defined as

$$\hat{R}_i = R_1 + \frac{R_2 - R_1}{N}(i-1), \quad i = 2,3...N+1 \tag{20}$$

and J_i^r is given by Eq. (16),

$$h_i = \frac{1}{2\alpha}\left[3N_z^s\left(\frac{\hat{R}_{i-1}}{\hat{R}_i}, \frac{t_1}{2\hat{R}_i}\right) - 1\right], \quad i = 2,3...N+1 \tag{21}$$

and, according to Eqs. (7) and (8), the shape factors are given by:

$$A_{cs}^j = A_{cs}\left(\frac{\hat{R}_1}{\hat{R}_{j-1}}, \frac{\hat{R}_1}{\hat{R}_j}\frac{t_1}{2\hat{R}_{j-1}}, \frac{t_1}{2\hat{R}_j}\right), \quad j = 2...N+1 \tag{22}$$

$$A_{ss}^{ij} = A_{ss}\left(\frac{\hat{R}_{i-1}}{\hat{R}_{j-1}}, \frac{\hat{R}_{i-1}}{\hat{R}_j}, \frac{\hat{R}_i}{\hat{R}_j}, \frac{\hat{R}_i}{\hat{R}_{j-1}}, \frac{t_1}{2\hat{R}_{j-1}}, \frac{t_1}{2\hat{R}_j}\right), \quad i = 2,3...N, \quad j = 3,4...N+1 \tag{23}$$

The normalized switching field is defined as the smallest (in absolute value) normalized field resulting in a local energy minimum with $\theta_1 = \theta_2 = ... = \theta_{N+1} = \pi$ while we gradually decrease the applied field from a large positive value and follow the local minimum originally located at $\theta_1 = \theta_2 = ... = \theta_{N+1} = 0$. Such defined switching field may coincide with normalized coercive field or normalized nucleation field but generally the switching field is different from them. In separate simulation runs, we vary t_2 (for the cylinder-cylinder structure) and R_2 (for the core-shell structure, see Fig. 1) while t_1 and R_1 are fixed. After substituting all parameters, including the dipolar coupling factors given by Eqs. (17), (18), (22), and (23), into Eqs. (14) or (19), and setting h and J_2 to selected values, we obtain the total energy as a function of $\theta_1, \theta_2, ..., \theta_{N+1}$ and we search for energy minima. It should be noted that A_{cc}, A_{cs}, A_{ss} are constants during this search.

Keeping an eye on technological requirements, we are interested in obtaining the switching field reduction without a significant loss of thermal stability. Since thermal stability is related to the energy barrier at zero applied field, both the switching field and the energy barrier have to be evaluated. For this purpose, the concept of "figure of merit" was defined in references [4,8] to be the ratio $m = \left[\Delta E(0)/H_{sw}\right]_{comp} / \left[\Delta E(0)/H_{sw}\right]_{spm}$, where the subscripts 'comp' and 'spm' stand for composite and single phase material, respectively. Assuming that the volume and saturation magnetization of the single phase material particle are $V = V_1 + V_2$ and $M_s = \left(M_1 V_1 + M_2 V_2\right)/\left(V_1 + V_2\right)$, respectively, we obtain $\left[\Delta E(0)/H_{sw}\right]_{spm} = 0.5\mu_0 M_s \left(V_1 + V_2\right)$ and, for both the two-spin and the multi-spin models, we obtain figures of merit for core-shell (m_{cs}) and conventional (m_{cc}) ECC particles as:

$$m_{cs} = \frac{\sigma^3}{\tau} \frac{\Delta e_{cs}(0)}{[\alpha\sigma^2 + (1-\sigma^2)]h_{sw,opt}} \tag{24}$$

$$m_{cc} = \frac{\Delta e_{cc}(0)}{(\alpha\rho_1 + \rho_2)h_{sw,opt}} \tag{25}$$

where σ is the ratio of the inner and outer radii of the shell, τ is the ratio of the shell height to the shell outer diameter, $\Delta e_{cs}(0)$ [$\Delta e_{cc}(0)$] is the normalized energy barrier of the core-shell [conventional] ECC particle for $h = 0$, $\rho_i = t_i/\left(2R_1\right)$, $i = 1,2$ and $h_{sw,opt}$ is the absolute value of the normalized optimum switching field. In Fig 3 (a-b), $h_{sw,opt}$ for each curve corresponds to the curve's minimum. From Eqs. (24) and (25), it is clear that among all $\left|h_{sw}\right|$, the optimal switching fields maximize the figures of merit. Using the multi-spin model, if the energy landscape Δe_{cc} for $h = 0$ has a maximum barrier height at point $\theta_1 = \theta_2 = ... = \theta_N = \pi/2$ (which may not be always true), then

$$\Delta e_{cc}(0) = \alpha\rho_1 h_1 + \rho_2 h_2 + 3\frac{A_{cc}(\rho_1, \rho_2, 0)}{R_1^3}. \tag{26}$$

If we neglect the magnetostatic interactions, then $\Delta e_{cc}(0) = \alpha\rho_1 h_1$ and m_{cc} will be identical to the figure of merit m in [8]. Before we can use Eqs. (24) and (25) to evaluate the figure of merit for various ECC particles, we must evaluate the optimum switching fields.

The results of the energy minimization for various J_2^r values using the six-spin model ($N = 5$) and for specific geometry parameters of core-shell and conventional particles are presented in Figs. 3a and 3b. Both figures display the normalized switching field versus the exchange coupling strength, J_1^r, for the core-shell ECC (Fig. 3a) and conventional ECC particle (Fig. 3b). For $J_2^r = 10$, the corresponding switching field curves nearly coincide with the switching field curves obtained from the respective two-spin models. To obtain a realistic exchange coupling strength that might correspond to $J_2^r = 10$, one can estimate that, if R_1 =3 nm and $\mu_0 M_1$ =0.7 T (saturation magnetization of some Co-based materials), J_2 =46.8 mJ/m^2 when $\alpha = 0.5$. The coupling strength parameter J_2 was estimated in [8] using the following formula:

$$J_2 = \frac{2A}{t}, \tag{27}$$

where A and t are the exchange constant and the spin region thickness, respectively. If we assume A =3·10^{-11} J/m (a value for Co used in OOMMF[17]) and t =3 nm, then, according to Eq. (27), J_2 =20 mJ/m^2 and if $\mu_0 M_1$ =0.7 T, then the corresponding $J_2^r = 4.3$.

If J_2^r goes to infinity, we can let $\theta_2 = \theta_3 = ... = \theta_{N+1}$ in the minimum search and the multi-spin model can be transformed to the two-spin model with only one dipolar coupling parameter and one exchange coupling parameter. In fact, if $\theta_2 = \theta_3 = ... = \theta_{N+1}$, then Eq. (14) transforms into:

$$e_{cc} = -\alpha\tau_1 h_1 \sin^2\theta_1 - \left(\tau_2 h_2 - \frac{3}{\alpha}\sum_{i=2}^{N}\sum_{j=i+1}^{N+1} A_{cc}^{ij}\right)\sin^2\theta_2 + (\sin\theta_1\sin\theta_2 - 2\cos\theta_1\cos\theta_2)\sum_{j=2}^{N+1} A_{cc}^{1j}$$
$$- 2h(\alpha\tau_1\cos\theta_1 + \tau_2\cos\theta_2) - 2J_1^r\cos(\theta_2 - \theta_1) - 2\sum_{i=1}^{N} J_i^r - \frac{2}{\alpha}\sum_{i=2}^{N}\sum_{j=i+1}^{N+1} A_{cc}^{ij} \tag{28}$$

It is not difficult to prove that

$$\tau_2 h_2 - \frac{3}{\alpha}\sum_{i=2}^{N}\sum_{j=i+1}^{N+1} A_{cc}^{ij} = \frac{\tau_2}{2\alpha}\left[3N_z(\tau_2) - 1\right], \tag{29}$$

where h_2 is defined in Eq. (15) and

$$\sum_{j=2}^{N+1} A_{cc}^{1j} = A_{cc}(\tau_1, \tau_2, 0)\,. \tag{30}$$

(Equations (29) and (30) are also used for the derivation of Eq. (26).)

Hence, the switching field curve for the multi-spin model with $J_2^r \to \infty$ coincides with that for the two-spin model with identical geometric and material parameters. Therefore, taking into account Eq. (27), it is unnecessarily complicated to use multi-spin model if *A* is large and *t* (thickness of the soft part) is small, since coherent rotation of magnetization in the soft part of the particle can be assumed. As J_2^r decreases, the corresponding switching field curve diverges away from the curve corresponding to the two-spin model while the optimum switching field increases (in absolute value). Thus, using multi-spin model is meaningful when dealing with materials with low exchange stiffness or ECC particles with large aspect ratios resulting in incoherent rotation or domain wall assisted switching.

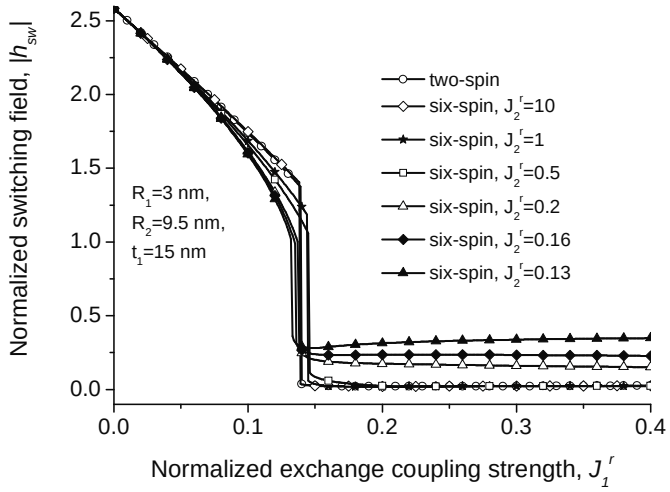

Fig. 3a Diagram of the normalized switching field versus the normalized exchange coupling strength J_1^r in the case of a core-shell ECC particle for the two-spin model and for various J_2^r in the six-spin model. Parameters R_1, R_2 and t_1 are fixed. The soft part of the particle is discretized.

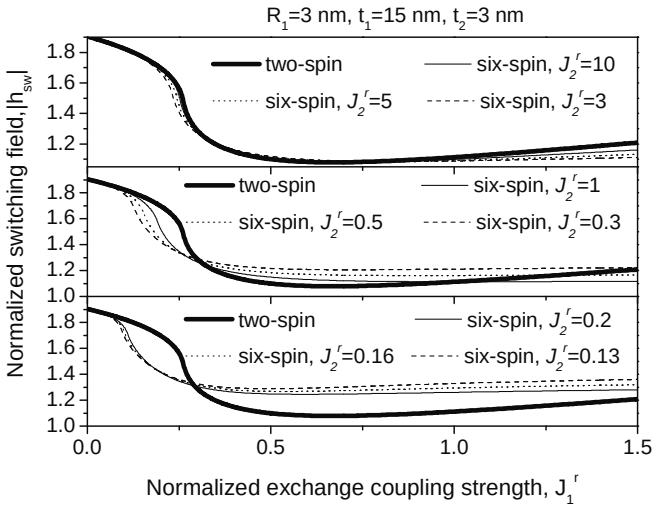

Fig. 3b Diagram of the normalized switching field versus the normalized exchange coupling strength J_1^r in the case of a conventional ECC particle for the two-spin model and for various J_2^r in the six-spin model. Parameters R_1, t_1 and t_2 are fixed. The soft part of the particle is discretized.

Figures 4(a,b) show the calculated normalized optimum switching fields $h_{sw,opt}$ for ECC particles of various geometries and of either type using the two-spin model. The $h_{sw,opt}$ profile for core-shell particles for a fixed t_1 decreases monotonically with increasing outer shell radius R_2. As R_2 increases, $h_{sw,opt}$ reaches a value close to zero (Fig. 4a). However, the dependence of $h_{sw,opt}$ for the conventional ECC particle on the soft cylinder height t_2 is different. As t_2 increases, $h_{sw,opt}$ first drops (at fixed t_1), reaching a minimum well above zero and then again increases, slowly approaching a limiting value. The lowest $h_{sw,opt}$ value belonging to the conventional ECC particle was reached for t_1=3 nm ($h_{sw,opt} = 0.33$). The curves of Fig. 4(a,b) are quite different from those reported in [18-19]. Both curves from [18-19] are monotonically decreasing with increasing soft layer thickness. The substantial differences in curve characteristics represent the fingerprint of the dipolar interaction effects. In fact, if we neglect the magnetostatic interactions ($A_{cc} = 0$ and $h_2 = 0$), then our model also predicts monotonically decreasing curves, just as those reported in [18-19].

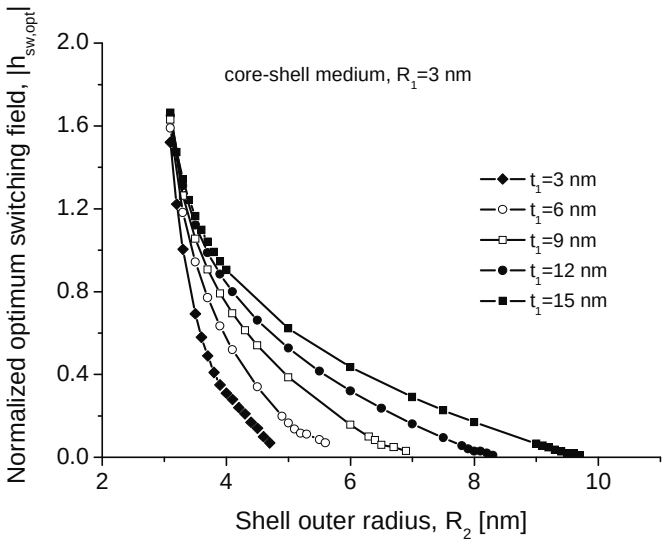

Fig. 4a Diagram of the normalized optimum switching field versus the outer radius of a core-shell ECC particle for various particle heights.

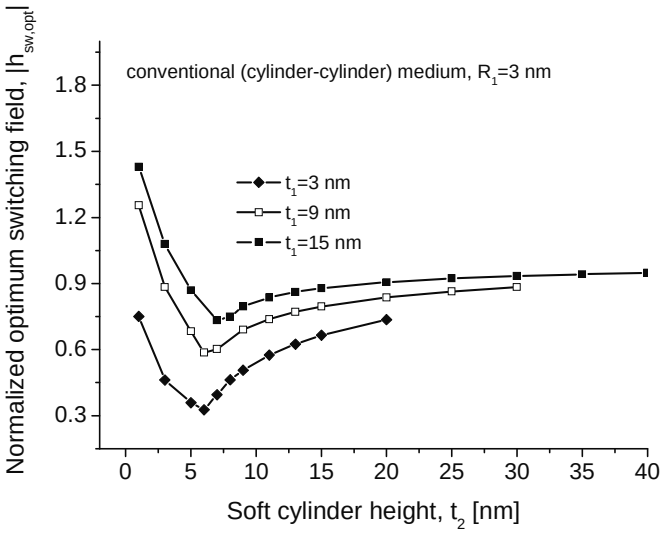

Fig. 4b Diagram of the normalized optimum switching field versus the soft cylinder height of a conventional ECC particle for various heights of the hard part.

Figures 5(a,b) show the figures of merit m_{cs} (a) and m_{cc} (b) for various particle geometries using the optimum switching field values taken from Fig. 4. The character of m_{cs} depends on t_1; however, in each m_{cs} profile at fixed t_1, the figure of merit reaches a maximum close to 2, which corresponds to $h_{sw,opt}$ close to zero. The larger t_1, the longer and lower the plateau is in the m_{cs} vs. R_2 curve. In the case of the conventional ECC particle, for a given t_1, values of m_{cc} reach a maximum for t_2 corresponding to the minimal $h_{sw,opt}$. In Ref. [8], the figure of merit does not exceed 2 whereas some m_{cc} values in our study do exceed 2. This difference in the figure of merit maxima again highlights the effects of magnetostatic interactions in the magnetic response of ECC particles.

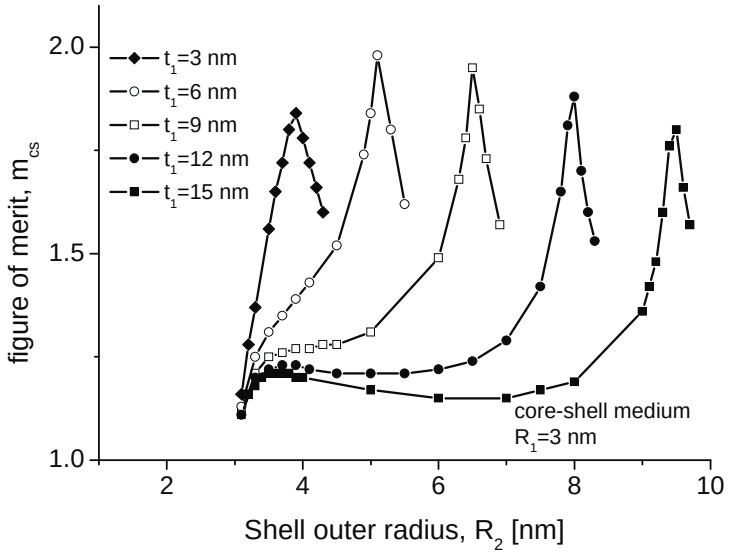

Fig. 5a Diagram of the figure of merit of a core-shell ECC particle versus the outer shell radius for various core-shell particle heights. The energy barrier and $\left|h_{sw,opt}\right|$ were calculated using the two-spin model.

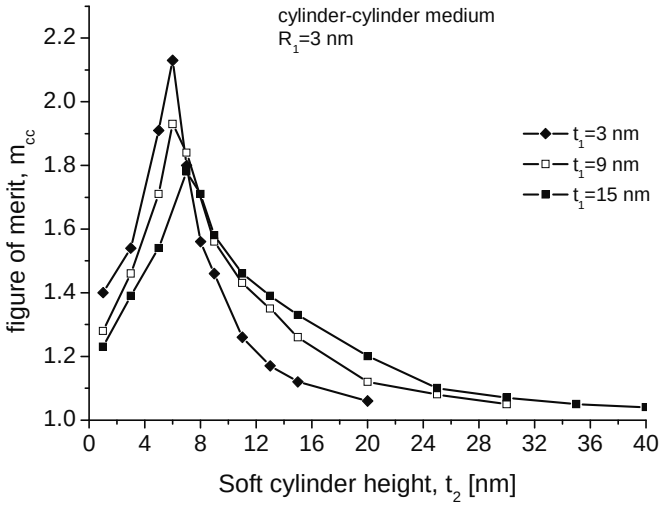

Fig. 5b Diagram of the figure of merit of a conventional (cylinder-cylinder) ECC particle versus the soft cylinder height for various hard cylinder heights. The energy barrier and $\left|h_{sw,opt}\right|$ were calculated using the two-spin model.

Conclusions

We have presented a multi-spin model for core-shell and conventional ECC particles, that takes into account the magnetostatic interactions among all the components. The key feature of our model is the opportunity to simulate quasi-analytically domain wall assisted switching. Our study is meaningful in particular when dealing with materials with low exchange stiffness or ECC particles with large aspect ratios. We have illustrated how the normalized switching field is influenced by the exchange coupling intrinsic to a given material. The geometry and the type of the ECC particle affect both the switching field and the zero-field energy barrier. While the switching field of a core-shell ECC particle approaches zero as the outer radius of the shell increases, a magnetization reversal of the conventional type occurs at a negative finite field. As for the ECC particle geometry associated with a figure of merit close to 2, the thickness of the soft layer is smaller in the case of the conventional ECC particle when comparing core-shell and conventional particle with an identical hard part. In the case of core-shell ECC particles, a figure of merit close to 2 corresponds to a switching field close to zero, which means that core-shell ECC particles can be of practical use when the hard part is highly anisotropic.

Acknowledgements

The work conducted in the Czech Republic and in Taiwan was supported by the Academy of Sciences of the Czech Republic and National Science Council within a Czech-Taiwanese Joint Research project. MDG acknowledges support from the US Department of Energy, Basic Energy Sciences, on contract number DE-FG02-01ER45893.

References:

[1] D. Suess, Appl. Phys. Lett. **89**, 113105 (2006).
[2] H. J. Richter, J. Phys. D: Appl. Phys. **40**, R149 (2007).
[3] V. Lomakin, R. Choi, B. Livshitz, S. Li, A. Inomata, and H.N. Bertram. Appl. Phys. Lett. **92**, 022502 (2008).
[4] R. H. Victora, and X. Shen, IEEE Trans. Magn. **41**, 537 (2005).
[5] R. H. Victora, and X. Shen, IEEE Trans. Magn. **41**, 2828 (2005).
[6] J. P. Wang, W. K. Shen, J. M. Bai, R. H. Victora, J. H. Judy, and W. L. Song, Appl. Phys. Lett. **86**, 142504 (2005).
[7] D. Goll, and S. Macke, Appl. Phys. Lett. **93**, 152512 (2008).

[8] H.J. Richter, and Yu. Dobin, J. Appl. Phys. **99**, 08Q905 (2006).
[9] A. Goncharov, T. Schrefl, G. Hrkac, J. Dean, S. Bance, D. Suess, O. Ertl, F. Dorfbauer, and J. Fidler, Appl. Phys. Lett. **91**, 222502 (2007).
[10] T.Tanaka, J.Matsuzaki, H.Kurisu, and S.Yamamoto, J. Magn. Magn. Mater. **320**, 3100 (2008).
[11] M. Beleggia, D. Vokoun, and M. De Graef, J. Magn. Magn. Mater. **321**, 1306 (2009).
[12] D. Vokoun, M. Beleggia, T. Rahman, H.C. Hou, and C.H. Lai, J. Appl. Phys. **103**, 7F520 (2008).
[13] E. C. Stoner, and E. P. Wohlfarth, Philos. Trans. R. Soc. London, Ser. A, **240**, 599 (1948).
[14] J.A. Nelder, and R. Mead, Computer Journal, **7**, 308 (1965).
[15] T. Shimatsu, T. Oikawa, Y. Inaba, H. Sato, I. Watanabe, H. Aoi, H. Muraoka, Y. Nakamura, IEEE Trans. on Magnetics **40**, 2461 (2004).
[16] M. Beleggia, M. De Graef, and Y.T. Millev, J. Phys. D: Appl. Phys. **39**, 891 (2006).
[17] http://math.nist.gov/oommf/
[18] D. Suess, J. Magn. Magn. Mater. **308**, 183 (2007).
[19] A.Y. Dobin, and H.J. Richter, Appl. Phys. Lett. **89**, 062512 (2006).